

Kapitza thermal resistance across individual grain boundaries in graphene

Khatereh Azizi^{a,b}, Petri Hirvonen^b, Zheyong Fan^{b,*}, Ari Harju^b, Ken R. Elder^c, Tapio Ala-Nissila^{b,d}, S. Mehdi Vaez Allaei^{a,e}

^aDepartment of Physics, University of Tehran, Tehran 14395-547, Iran

^bCOMP Centre of Excellence, Department of Applied Physics, Aalto University School of Science, P.O. Box 11000, FIN-00076 Aalto, Espoo, Finland

^cDepartment of Physics, Oakland University, Rochester, Michigan 48309, USA

^dDepartments of Mathematical Sciences and Physics, Loughborough University, Loughborough, Leicestershire LE11 3TU, UK

^eSchool of Physics, Institute for Research in Fundamental Sciences (IPM), Tehran 19395-5531, Iran

Abstract

We study heat transport across individual grain boundaries in suspended monolayer graphene using extensive classical molecular dynamics (MD) simulations. We construct bicrystalline graphene samples containing grain boundaries with symmetric tilt angles using the two-dimensional phase field crystal method and then relax the samples with MD. The corresponding Kapitza resistances are then computed using nonequilibrium MD simulations. We find that the Kapitza resistance depends strongly on the tilt angle and shows a clear correlation with the average density of defects in a given grain boundary, but is not strongly correlated with the grain boundary line tension. We also show that quantum effects are significant in quantitative determination of the Kapitza resistance by applying the mode-by-mode quantum correction to the classical MD data. The corrected data are in good agreement with quantum mechanical Landauer-Bütticker calculations.

Keywords: Grain boundary, Kapitza resistance, Graphene, Molecular dynamics, Phase field crystal

1. Introduction

Graphene [1], the famous two-dimensional allotrope of carbon, has been demonstrated to have extraordinary electronic [2], mechanical [3], and thermal [4] properties in its pristine form. However, large-scale graphene films, which are needed for industrial applications are typically grown by chemical vapor deposition [5] and are polycrystalline in nature [6], consisting of domains of pristine graphene with varying orientations separated by grain boundaries (GB) [7–9]. They play a significant or even dominant role in influencing many properties of graphene [10, 11].

One of the most striking properties of pristine graphene is its extremely high heat conductivity, which has been shown to be in excess of 5000 W/mK [4, 12]. Grain boundaries in graphene act as line defects or one-dimensional interfaces which leads to a strong reduction of the heat conductivity in multigrain samples [13, 14]. The influence of GBs can be quantified by the Kapitza or thermal boundary resistance R . The Kapitza resistance of graphene grain boundaries has been previously computed using molecular dynamics (MD) [15, 16] and Landauer-Bütticker [17, 18] methods, and has also been measured experimentally [19]. However, these works have only considered a few separate tilt angles, and a systematic investigation on the dependence of the Kapitza resistance on the tilt angle between any two pristine grains is still lacking. The relevant questions here concern both the magnitude R for different tilt angles and

possible correlations between the structure or line tension of the GBs and the corresponding value of R .

Modelling realistic graphene GBs has remained a challenge due to the multiple length and time scales involved. Recently, an efficient multiscale approach [20] for modelling polycrystalline graphene samples was developed based on phase field crystal (PFC) models [21, 22]. The PFC models are a family of continuum methods for modelling the atomic level structure and energetics of crystals, and their evolution at diffusive time scales (as compared to vibrational time scales in MD). The PFC models retain full information about the atomic structure and elasticity of the solid [22]. It has been shown [20] that using the PFC approach in two-dimensional space one can obtain large, realistic and locally relaxed microstructures that can be mapped to atomic coordinates for further relaxation in three-dimensional space with the usual atomistic simulation methods.

In this work, we employ the multiscale PFC strategy of Ref. [20] to generate large samples of tilted, bicrystalline graphene with a well-defined GB between the two grains. These samples are then further relaxed with MD at $T = 300$ K. A heat current is generated across the bicrystals using nonequilibrium MD (NEMD) simulations, and the Kapitza resistance is computed from the temperature drop across the GB. We map the values of $R(\theta)$ for a range of different tilt angles θ and demonstrate how R correlates with the structure of the GBs. Finally, we demonstrate that quantum corrections need to be included in R to obtain quantitative agreement with experiments and lattice dynamical calculations.

*Corresponding author. E-mail: brucenju@gmail.com (Zheyong Fan)

Email addresses: petri.hirvonen@aalto.fi (Petri Hirvonen), smvaez@ut.ac.ir (S. Mehdi Vaez Allaei)

2. Models and Methods

2.1. PFC models

PFC approaches typically employ a classical density field $\psi(\mathbf{r})$ to describe the systems. The ground state of ψ is governed by a free energy functional $F[\psi(\mathbf{r})]$ that is minimized either by a periodic or a constant ψ , corresponding to crystalline and liquid states, respectively. We use the standard PFC model

$$F = \int d\mathbf{r} \left(\frac{1}{2} \psi \left[\epsilon + (q^2 + \nabla^2)^2 \right] \psi + \frac{1}{3} \tau \psi^3 + \frac{1}{4} \psi^4 \right), \quad (1)$$

where the model parameters ϵ and τ are phenomenological parameters related to temperature and average density, respectively. The component $(q^2 + \nabla^2)^2$ penalizes for deviations from the length scale set by the wave number q , giving rise to a spatially oscillating ψ and to elastic behaviour [21, 22]. The crystal structure in the ground state is dictated by the formulation of F and the average density of ψ , and for certain parameter values the ground state of ψ displays a honeycomb lattice of density maxima as appropriate for graphene [20].

The PFC calculations are initialized with symmetrically tilted 2-crystals in a periodic, two-dimensional computational unit cell. The initial guess for the crystalline grains is obtained by using the one-mode approximation [22]

$$\psi(x, y) = \cos(qx) \cos\left(\frac{qy}{\sqrt{3}}\right) - \frac{1}{2} \cos\left(\frac{2qy}{\sqrt{3}}\right), \quad (2)$$

and by rotating alternately by $\pm\theta$. The tilt angle between two adjacent grains is $\theta - (-\theta) = 2\theta$, which ranges from $2\theta = 0^\circ$ to $2\theta = 60^\circ$ (see Fig. 1 for examples). We consider a subset of the tilt angles investigated in Ref. [20], with the exact values being listed in Table 1. The rotated grains and the unit cell size are matched together as follows: if just one of the rotated grains filled the whole unit cell, it would be perfectly continuous at the periodic edges. Along both interfaces, narrow strips a few atomic spacings wide are set to the average density – corresponding to a disordered state – to give the grain boundaries some additional freedom to find their lowest-energy configuration. We assume non-conserved dynamics to relax the systems in analogy to chemical vapour deposition [23] – the number of atoms in the monolayer can vary as if due to exchange with a vapor phase. In addition, the unit cell dimensions are allowed to vary to minimize strain. Further details of the PFC calculations can be found in Ref. [20]. The relaxed density field is mapped to a discrete set of atomic coordinates suited for the initialization of MD simulations [20].

2.2. NEMD simulations

We use the NEMD method as implemented in the GPUMD (graphics processing units molecular dynamics) code [24–26] to calculate the Kapitza resistance, using the Tersoff [27] potential with optimized parameters [28] for graphene. The initial structures obtained by the PFC method are rescaled by an appropriate factor to have zero in-plane stress at 300 K in the MD simulations with the optimized Tersoff potential [28].

In the NEMD simulations, periodic boundary conditions are applied in the transverse direction, whereas fixed boundary conditions are applied in the transport direction. We first equilibrate the system at 1 K for 1 ns, then increase the temperature from 1 K to 300 K during 1 ns, and then equilibrate the system at 300 K for 1 ns. After these steps, we apply a Nosé-Hoover chain of thermostats [29–31] to the heat source and sink, choosing as two blocks of atoms around the two ends of the system, as schematically shown in Fig. 2. The temperatures of the heat source and sink are maintained at 310 K and 290 K, respectively. We have checked that steady state can be well established within 5 ns. In view of this, we calculate the temperature profile $T(x)$ of the system and the energy exchange rate Q between the system and the thermostats using data sampled in another 5 ns. The velocity-Verlet integration scheme [32] with a time step of 1 fs is used for all the calculations. Three independent calculations are performed for each system and the error estimates reported in Table 1 correspond to the standard error of the independent results.

In steady state, apart from the nonlinear regions around the heat source and the sink intrinsic to the method, a linear temperature profile can be established on each side of the GB, but with an inherent discontinuity (temperature jump) at the GB. An example of this for the system with $2\theta = 9.43^\circ$ is shown in Fig. 3. The Kapitza resistance R is defined as the ratio of the temperature jump ΔT and the heat flux J across the grain boundary:

$$R = \frac{\Delta T}{J}, \quad (3)$$

where J can be calculated from the energy exchange rate Q (between the system and thermostat) and the cross-sectional area S (graphene thickness is chosen as 0.335 nm in our calculations), *i.e.* $J = Q/S$.

3. Results and Discussion

It is well known [15, 16, 33] that the calculated Kapitza resistance depends on the sample length in NEMD simulations. Figure 4 shows the calculated Kapitza resistance R in the $2\theta = 9.43^\circ$ case as a function of the sample length L_x . Using fixed boundary conditions as described above, R saturates at around $L_x = 400$ nm. On the other hand, using periodic boundaries as described in Ref. [15], R converges more slowly. To this end, we have here used fixed boundary conditions and a sample length of 400 nm for all the systems. The calculated temperature jump ΔT , heat flux J , and Kapitza resistance R in the 13 bicrystalline systems are listed in Table 1.

The Kapitza resistance calculated from the heat flux does not contain any information on the contributions from individual phonon modes. Methods of spectral decomposition of both the heat current (flux) [37–42] and the temperature [43] within the NEMD framework have been developed recently. Here, we use the spectral decomposition formalism as described in Ref. [42] to calculate the spectral conductance $g(\omega)$ of the $2\theta = 9.43^\circ$ system. In this method, one first calculates the following nonequilibrium heat current correlation function (t is the correlation

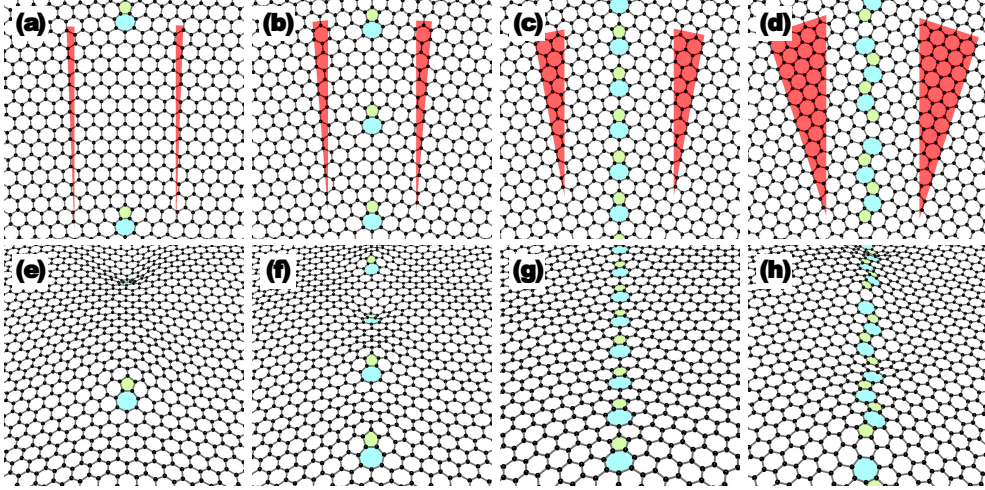


Figure 1: A schematic illustration of the definition of the tilt angle in bicrystalline graphene with symmetrically tilted grain boundaries. (a)-(d): Grain boundary with tilt angles (indicated by the red wedges) of $2\theta = 4.42^\circ, 9.43^\circ, 21.79^\circ,$ and 36.52° before MD relaxation. (e)-(h): the corresponding systems after MD relaxation. For clarity, only the small part close to the grain boundary is shown for each system; the sample size in our NEMD simulations is much larger, which is $L_x = 400$ nm (transport direction) and $L_y = 25$ nm (transverse direction). (A colour version of this figure can be viewed online.)

Table 1: The GB tilt angle 2θ , the corresponding temperature jump ΔT , heat flux J , Kapitza resistance R , Kapitza length L_K , grain boundary line tension γ , and defect density ρ for the 13 bicrystalline graphene samples considered here.

2θ ($^\circ$)	ΔT (K)	J (GW/m 2)	R (m 2 K/GW)	L_K (nm)	γ (eV/nm)	ρ (1/nm)
1.10	0.09 ± 0.07	51.3 ± 0.4	0.0018 ± 0.0013	10 ± 7	0.55	0.08
4.41	0.73 ± 0.14	50.4 ± 0.6	0.0144 ± 0.0026	75 ± 13	2.21	0.31
9.43	1.36 ± 0.15	45.7 ± 0.3	0.0298 ± 0.0033	155 ± 17	3.84	0.67
13.17	1.62 ± 0.08	48.1 ± 0.5	0.0337 ± 0.0020	175 ± 10	4.71	0.93
18.73	1.99 ± 0.06	43.9 ± 0.2	0.0453 ± 0.0015	236 ± 8	5.02	1.32
21.79	1.97 ± 0.01	47.8 ± 0.2	0.0412 ± 0.0004	214 ± 2	4.69	1.54
27.80	2.39 ± 0.04	43.6 ± 0.3	0.0548 ± 0.0005	285 ± 3	4.71	1.95
32.20	2.49 ± 0.10	43.4 ± 0.7	0.0574 ± 0.0033	298 ± 17	3.77	2.25
36.52	2.48 ± 0.14	43.9 ± 0.5	0.0565 ± 0.0026	294 ± 14	4.93	1.91
42.10	2.30 ± 0.02	43.1 ± 0.2	0.0534 ± 0.0006	278 ± 3	5.50	1.46
46.83	1.93 ± 0.06	46.4 ± 0.3	0.0416 ± 0.0014	216 ± 7	5.16	1.06
53.60	1.01 ± 0.06	41.2 ± 0.3	0.0245 ± 0.0014	127 ± 7	3.36	0.52
59.04	0.17 ± 0.07	47.3 ± 0.1	0.0036 ± 0.0014	19 ± 7	0.61	0.08

time):

$$K(t) = \sum_{i \in A} \sum_{j \in B} \left\langle \frac{\partial U_i(0)}{\partial \vec{r}_{ij}} \cdot \vec{v}_j(t) - \frac{\partial U_j(0)}{\partial \vec{r}_{ji}} \cdot \vec{v}_i(t) \right\rangle, \quad (4)$$

where U_i and \vec{v}_i are respectively the potential energy and velocity of particle i , $\vec{r}_{ij} = \vec{r}_j - \vec{r}_i$ (\vec{r}_i is the position of particle i), and $K(t = 0)$ measures the heat current flowing from a block A to an adjacent block B arranged along the transport direction. Then, one performs a Fourier transform to get the spectral conductance:

$$g(\omega) = \frac{2}{S \Delta T} \int_{-\infty}^{+\infty} dt e^{i\omega t} K(t). \quad (5)$$

The spectral conductance is normalized as

$$G = \int_0^\infty \frac{d\omega}{2\pi} g(\omega), \quad (6)$$

where G is the total Kapitza conductance (also called thermal boundary conductance), which is the inverse of the Kapitza resistance $G = 1/R$.

Figure 5(a) shows the calculated correlation function $K(t)$, which resembles the velocity autocorrelation function whose Fourier transform is the phonon density of states [44]. Indeed, thermal conductance in the quasi-ballistic regime is intimately related to the phonon density of states. The corresponding spectral conductance $g(\omega)$ is shown as the solid line in Fig. 5(b). The total thermal boundary conductance is $G \approx 33$ GW/m 2 /K, corresponding to a Kapitza resistance of $R \approx 0.03$ m 2 /GW.

In view of the high Debye temperature (around 2000 K) for pristine graphene [45], we expect that it is necessary to correct the classical results to properly account for possible quantum effects. While using classical statistics can lead to [46] an underestimate of the scattering time for the low-frequency

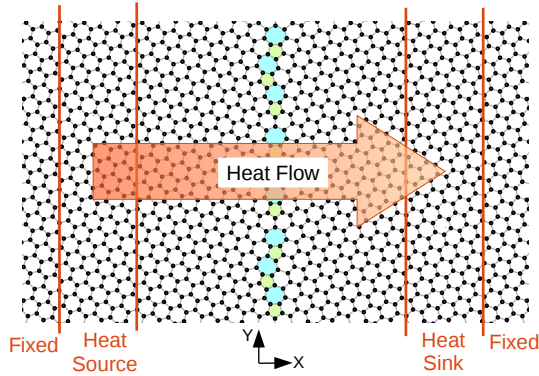


Figure 2: A schematic illustration of the NEMD setup used in computing the Kapitza resistance. (A colour version of this figure can be viewed online.)

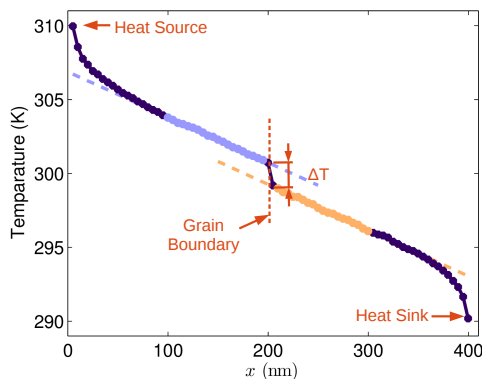


Figure 3: A typical steady-state temperature profile in bicrystalline graphene with a tilt angle of $2\theta = 9.43^\circ$. On each side of the grain boundary, excluding the nonlinear region around the heat source or the sink, one can fit the temperature by a linear function and then extract the temperature jump as the difference between the two linear functions at the grain boundary [15, 16, 33–36]. (A colour version of this figure can be viewed online.)

phonons as well as an overestimate of the heat capacity of the high-frequency phonons for thermal transport in the diffusive regime, only the second effect matters here in the quasi-ballistic regime. Therefore, one can correct the results by multiplying the classical spectral conductance by the ratio of the quantum heat capacity to the classical one: $x^2 e^x / (e^x - 1)^2$, where $x = \hbar\omega / k_B T$, with \hbar , k_B , T being the Planck constant, Boltzmann constant, and system temperature, respectively. This factor is unity in the low-frequency (high-temperature) limit and zero in the high-frequency (low-temperature) limit. Applying this mode-to-mode quantum correction to the classical spectral conductance gives the quantum spectral conductance represented by the dashed line in Fig. 5(b). The integral of the quantum corrected spectral conductance is reduced by a factor of about 2.3 as compared to the classical one.

Figure 6(a) shows the calculated Kapitza resistances for all the 13 systems as a function of the tilt angle, both before (red squares) and after (blue circles) applying the quantum correction. It clearly shows that the Kapitza resistance depends

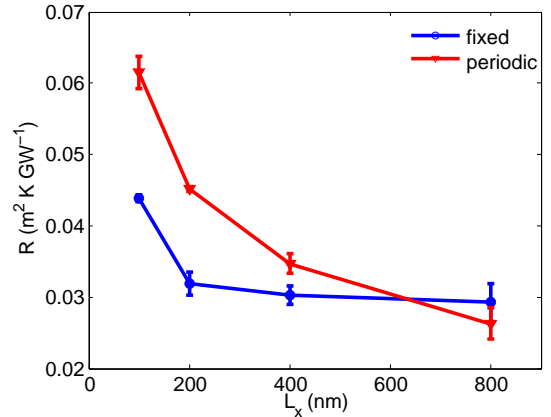


Figure 4: Kapitza resistance as a function of the sample length L_x obtained by using fixed boundary conditions (circles) and periodic boundaries (triangles) in the case of $2\theta = 9.43^\circ$. (A colour version of this figure can be viewed online.)

strongly on the tilt angle, varying by more than one order of magnitude. The Kapitza resistance increases monotonically from both sides to the middle angle of $2\theta \sim 30^\circ$, except for one “anomalous” system with $2\theta = 21.79^\circ$. This system has smaller R than that with $2\theta = 18.73^\circ$. One intuitive explanation is that this system is relatively flat compared to other systems, as can be seen from Figs. 1(e)-(h). Similar “anomalous” heat transport has been reported in Ref. [47] for the same grain boundary tilt angle.

The largest Kapitza resistances occurring around the intermediate angles, being about $0.12 \text{ m}^2/\text{K}/\text{GW}$ after quantum corrections, are more than an order of magnitude smaller than those in grain boundaries in silicon nanowires [36]. A more reasonable comparison between different materials is in terms of the Kapitza length L_K [48], defined as the system length of the corresponding pristine material at which the bulk thermal resistance due to phonon-phonon scattering equals the Kapitza resistance. Mathematically, we have

$$L_K = \kappa R, \quad (7)$$

where κ is the thermal conductivity of the bulk material. We calculate L_K by assuming a value of $\kappa = 5200 \text{ W/mK}$ for pristine graphene according to the very recent experiments [12] and list the values in Table 1. The largest Kapitza lengths (corresponding to the largest Kapitza resistances) before quantum corrections are about 300 nm, which would be about 700 nm after quantum corrections. These values are actually larger than those for silicon nanowires. Therefore, the effect of grain boundaries on heat transport in graphene is not small even though the Kapitza resistances are relatively small.

To facilitate comparison with previous works, we also show the Kapitza conductances in Fig. 6(b). The Kapitza conductances in our systems range from about $17 \text{ GW}/\text{m}^2/\text{K}$ to more than $500 \text{ GW}/\text{m}^2/\text{K}$ before applying the quantum corrections. Bagri *et al.* [15] reported Kapitza conductance values (obtained by NEMD simulations with periodic boundary conditions in the transport direction) ranging from $15 \text{ GW}/\text{m}^2/\text{K}$ to

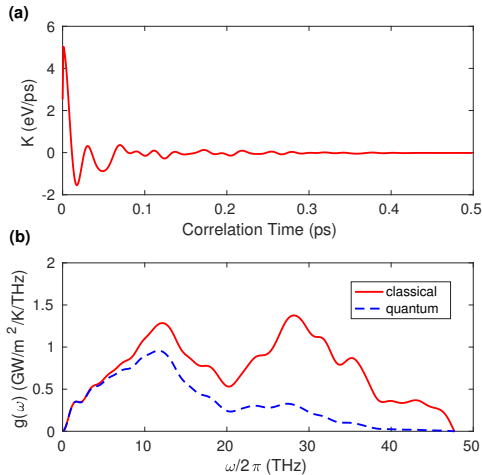


Figure 5: (a) The nonequilibrium heat current correlation function $K(t)$ as a function of correlation time. (b) The spectral conductance before (solid line) and after (dashed line) mode-to-mode quantum corrections as a function of the phonon frequency. The system considered here corresponds to the case of $2\theta = 9.43^\circ$, but similar results are obtained for all other cases. (A colour version of this figure can be viewed online.)

45 $\text{GW}/\text{m}^2/\text{K}$. The lower limit of 15 $\text{GW}/\text{m}^2/\text{K}$ does not conflict with our data, as this value is reported in a system of a grain size of 25 nm, where the data cannot have converged yet. On the other hand, Cao and Qu (obtained by NEMD simulations with fixed boundary conditions in the transport direction) [16] reported saturated Kapitza conductance values in the range of 19 – 47 $\text{GW}/\text{m}^2/\text{K}$, which fall well within the values that we obtained. Last, we note that quantum mechanical Landauer-Bütticker calculations by Serov *et al.* [18] predicted the Kapitza conductance to be about 8 $\text{GW}/\text{m}^2/\text{K}$ for graphene grain boundaries comparable to those in our samples with intermediate tilt angles ($2\theta \sim 30^\circ$). This is much smaller than the classical Kapitza conductances (about 20 $\text{GW}/\text{m}^2/\text{K}$), but agree well with our quantum corrected values. This comparison justifies the mode-to-mode quantum correction we applied to the classical data and resolves the discrepancy between the results from classical NEMD simulations and quantum mechanical Landauer-Bütticker calculations.

The last remaining issue concerns the possible correlation of the values of $R(\theta)$ with the energetics and structure of the GBs. The grain boundary line tension and the defect density are closely related to the tilt angle. The line tension γ is defined as

$$\gamma = \lim_{L_y \rightarrow \infty} \frac{\Delta E}{L_y}, \quad (8)$$

in the thermodynamic limit, where ΔE is the formation energy for a GB of length L_y . The defect density is defined as

$$\rho = \frac{N_{\text{p-h}}}{L_y}, \quad (9)$$

where $N_{\text{p-h}}$ is the number of pentagon-heptagon pairs in the grain boundary. The calculated γ and ρ values for all the tilt an-

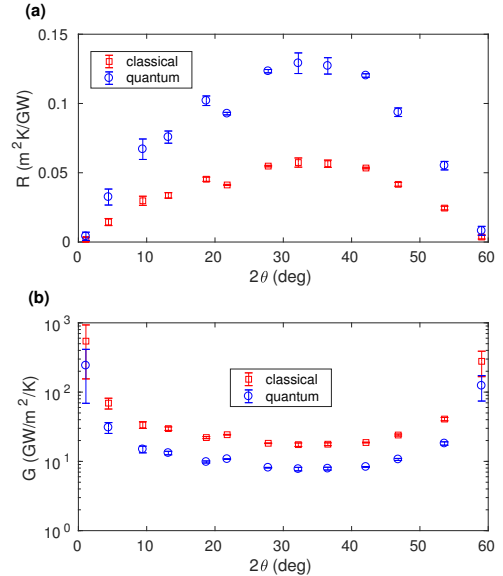


Figure 6: (a) Kapitza resistance R of the grain boundary before (labeled as “classical”) and after (labeled as “quantum”) the mode-to-mode quantum correction as a function of the tilt angle 2θ . (b) The corresponding Kapitza conductance G as a function of the tilt angle. (A colour version of this figure can be viewed online.)

gles are listed in Table 1 and plotted in Figs. 7(a)-(b). In Figs. 7(c)-(d), we plot the Kapitza resistance against γ and ρ , respectively. At small and large tilt angles, where the defect density is relatively small, there is a clear linear dependence of R on both γ and ρ . However, at intermediate tilt angles ($2\theta \approx 30^\circ$), where the defect density is relatively large, the linear dependences become less clear, especially between R and γ , which may indicate increased interactions between the defects. Overall, there is a stronger correlation between the Kapitza resistance and the defect density which is consistent with the idea of enhanced phonon scattering with increasing ρ .

4. Summary and Conclusions

In summary, we have employed an efficient multiscale modeling strategy based on the PFC approach and atomistic MD simulations to systematically evaluate the Kapitza resistances in graphene grain boundaries for a wide range of tilt angles between adjacent grains. Strong correlations between the Kapitza resistance and the tilt angle, the grain boundary line tension, and the defect density are identified. Quantum effects, which have been ignored in previous studies, are found to be significant. By applying a mode-to-mode quantum correction method based on spectral decomposition, we have demonstrated that good agreement between the classical molecular dynamics data and the quantum mechanical Landauer-Bütticker method can be obtained.

We emphasize that we have only considered suspended systems in this work. In a recent experimental work by Yasaei *et al.* [19], Kapitza conductances (inverse of the Kapitza resis-

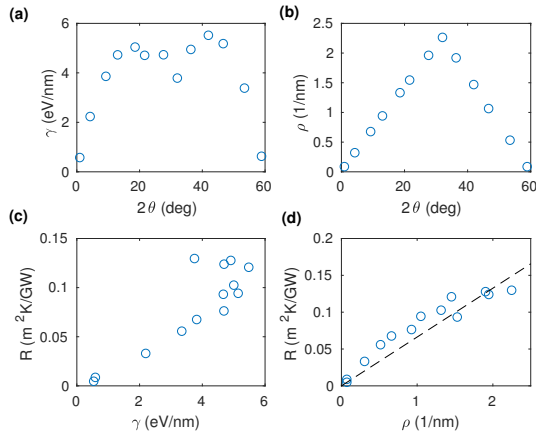


Figure 7: (a) The grain boundary line tension γ and (b) the defect density ρ versus the tilt angle 2θ . (c) and (d) The quantum corrected Kapitza resistance R versus γ and ρ , respectively. The dashed line in (d) is a guide to the eye. (A colour version of this figure can be viewed online.)

tance) for a few supported (on SiN substrate) samples containing grain boundaries with different tilt angles were measured. The Kapitza conductances reported in this work are about one order of magnitude smaller than our quantum corrected values. This large discrepancy indicates that certain substrates may strongly affect heat transport across graphene grain boundaries and more work is needed to clarify this.

Acknowledgements

This research has been supported by the Academy of Finland through its Centres of Excellence Program (Project No. 251748). We acknowledge the computational resources provided by Aalto Science-IT project and Finland's IT Center for Science (CSC). K.A. acknowledges financial support from the Ministry of Science and Technology of Islamic Republic of Iran. P.H. acknowledges financial support from the Foundation for Aalto University Science and Technology, and from the Vilho, Yrjö and Kalle Väisälä Foundation of the Finnish Academy of Science and Letters. Z.F. acknowledges the support of the National Natural Science Foundation of China (Grant No. 11404033). K.R.E. acknowledges financial support from the National Science Foundation under Grant No. DMR-1506634.

References

[1] K. S. Novoselov, A. K. Geim, S. V. Morozov, D. Jiang, Y. Zhang, S. V. Dubonos, I. V. Grigorieva, A. A. Firsov, Electric field effect in atomically thin carbon films, *Science* 306 (5696) (2004) 666–669. [arXiv:http://science.sciencemag.org/content/306/5696/666.full.pdf](http://science.sciencemag.org/content/306/5696/666.full.pdf), doi:10.1126/science.1102896. URL <http://science.sciencemag.org/content/306/5696/666>

[2] A. H. Castro Neto, F. Guinea, N. M. R. Peres, K. S. Novoselov, A. K. Geim, The electronic properties of graphene, *Rev. Mod. Phys.* 81 (2009) 109–162. doi:10.1103/RevModPhys.81.109. URL <https://link.aps.org/doi/10.1103/RevModPhys.81.109>

[3] C. Lee, X. Wei, J. W. Kysar, J. Hone, Measurement of the elastic properties and intrinsic strength of monolayer graphene, *Science* 321 (5887) (2008) 385–388. [arXiv:http://science.sciencemag.org/content/321/5887/385.full.pdf](http://science.sciencemag.org/content/321/5887/385.full.pdf), doi:10.1126/science.1157996. URL <http://science.sciencemag.org/content/321/5887/385>

[4] A. A. Balandin, S. Ghosh, W. Bao, I. Calizo, D. Teweldebrhan, F. Miao, C. N. Lau, Superior thermal conductivity of single-layer graphene, *Nano Letters* 8 (3) (2008) 902–907. [arXiv:http://dx.doi.org/10.1021/nl0731872](http://dx.doi.org/10.1021/nl0731872), doi:10.1021/nl0731872. URL <http://dx.doi.org/10.1021/nl0731872>

[5] X. Li, W. Cai, J. An, S. Kim, J. Nah, D. Yang, R. Piner, A. Velamakanni, I. Jung, E. Tutuc, S. K. Banerjee, L. Colombo, R. S. Ruoff, Large-area synthesis of high-quality and uniform graphene films on copper foils, *Science* 324 (5932) (2009) 1312–1314. [arXiv:http://science.sciencemag.org/content/324/5932/1312.full.pdf](http://science.sciencemag.org/content/324/5932/1312.full.pdf), doi:10.1126/science.1171245. URL <http://science.sciencemag.org/content/324/5932/1312>

[6] P. Huang, C. Ruiz-Vargas, A. V. D. Zande, W. Whitney, M. Levendorf, J. Kevek, S. Garg, J. Alden, C. Husted, Y. Zhu, J. Park, P. McEuren, D. Muller, Grains and grain boundaries in single-layer graphene atomic patchwork quilts, *Nature* 469 (2011) 389 – 392. URL <http://dx.doi.org/10.1038/nature09718>

[7] O. V. Yazyev, S. G. Louie, Topological defects in graphene: Dislocations and grain boundaries, *Phys. Rev. B* 81 (2010) 195420. doi:10.1103/PhysRevB.81.195420. URL <https://link.aps.org/doi/10.1103/PhysRevB.81.195420>

[8] T.-H. Liu, G. Gajewski, C.-W. Pao, C.-C. Chang, Structure, energy, and structural transformations of graphene grain boundaries from atomistic simulations, *Carbon* 49 (7) (2011) 2306 – 2317. doi:http://dx.doi.org/10.1016/j.carbon.2011.01.063. URL <http://www.sciencedirect.com/science/article/pii/S0008622311000911>

[9] Y. Liu, B. I. Yakobson, Cones, pringles, and grain boundary landscapes in graphene topology, *Nano Letters* 10 (6) (2010) 2178–2183, pMID: 20481585. [arXiv:http://dx.doi.org/10.1021/nl100988r](http://dx.doi.org/10.1021/nl100988r), doi:10.1021/nl100988r. URL <http://dx.doi.org/10.1021/nl100988r>

[10] O. V. Yazyev, Y. P. Chen, Polycrystalline graphene and other two-dimensional materials, *Nat. Nanotech.* 9 (2014) 755 – 767. URL <http://dx.doi.org/10.1038/nnano.2014.166>

[11] A. W. Cummings, D. L. Duong, V. L. Nguyen, D. Van Tuan, J. Kotakoski, J. E. Barrios Vargas, Y. H. Lee, S. Roche, Charge transport in polycrystalline graphene: Challenges and opportunities, *Advanced Materials* 26 (30) (2014) 5079–5094. doi:10.1002/adma.201401389. URL <http://dx.doi.org/10.1002/adma.201401389>

[12] T. Ma, Z. Liu, J. Wen, Y. Gao, X. Ren, H. Chen, C. Jin, X.-L. Ma, N. Xu, H.-M. Cheng, W. Ren, Tailoring the thermal and electrical transport properties of graphene films by grain size engineering, *Nature Communications* 8 (2017) 14486. URL <http://dx.doi.org/10.1038/ncomms14486>

[13] K. R. Hahn, C. Melis, L. Colombo, Thermal transport in nanocrystalline graphene investigated by approach-to-equilibrium molecular dynamics simulations, *Carbon* 96 (2016) 429 – 438. doi:http://dx.doi.org/10.1016/j.carbon.2015.09.070. URL <http://www.sciencedirect.com/science/article/pii/S0008622315302888>

[14] Z. Fan, L. F. C. Pereira, P. Hirvonen, M. M. Ervasti, K. R. Elder, D. Donadio, A. Harju, T. Ala-Nissila, Bimodal grain-size scaling of thermal transport in polycrystalline graphene from large-scale molecular dynamics simulations, Unpublished.

[15] A. Bagri, S.-P. Kim, R. S. Ruoff, V. B. Shenoy, Thermal transport across twin grain boundaries in polycrystalline graphene from nonequilibrium molecular dynamics simulations, *Nano Letters* 11 (9) (2011) 3917–3921, pMID: 21863804. [arXiv:http://dx.doi.org/10.1021/nl202118d](http://dx.doi.org/10.1021/nl202118d), doi:10.1021/nl202118d. URL <http://dx.doi.org/10.1021/nl202118d>

[16] A. Cao, J. Qu, Kapitza conductance of symmetric tilt grain boundaries in graphene, *Journal of Applied Physics* 111 (5) (2012) 053529.

- arXiv:<http://dx.doi.org/10.1063/1.3692078>, doi:10.1063/1.3692078.
URL <http://dx.doi.org/10.1063/1.3692078>
- [17] Y. Lu, J. Guo, Thermal transport in grain boundary of graphene by non-equilibrium greens function approach, *Applied Physics Letters* 101 (4) (2012) 043112. arXiv:<http://dx.doi.org/10.1063/1.4737653>, doi:10.1063/1.4737653.
URL <http://dx.doi.org/10.1063/1.4737653>
- [18] A. Y. Serov, Z.-Y. Ong, E. Pop, Effect of grain boundaries on thermal transport in graphene, *Applied Physics Letters* 102 (3) (2013) 033104. arXiv:<http://dx.doi.org/10.1063/1.4776667>, doi:10.1063/1.4776667.
URL <http://dx.doi.org/10.1063/1.4776667>
- [19] P. Yasaei, A. Fathizadeh, R. Hantehzadeh, A. K. Majee, A. El-Ghandour, D. Estrada, C. Foster, Z. Aksamija, F. Khalili-Araghi, A. Salehi-Khojin, Bimodal phonon scattering in graphene grain boundaries, *Nano Letters* 15 (7) (2015) 4532–4540, pMID: 26035002. arXiv:<http://dx.doi.org/10.1021/acs.nanolett.5b01100>, doi:10.1021/acs.nanolett.5b01100.
URL <http://dx.doi.org/10.1021/acs.nanolett.5b01100>
- [20] P. Hirvonen, M. M. Ervasti, Z. Fan, M. Jalalvand, M. Seymour, S. M. Vaez Allaei, N. Provatas, A. Harju, K. R. Elder, T. Ala-Nissila, Multiscale modeling of polycrystalline graphene: A comparison of structure and defect energies of realistic samples from phase field crystal models, *Phys. Rev. B* 94 (2016) 035414. doi:10.1103/PhysRevB.94.035414.
URL <https://link.aps.org/doi/10.1103/PhysRevB.94.035414>
- [21] K. R. Elder, M. Katakowski, M. Haataja, M. Grant, Modeling elasticity in crystal growth, *Phys. Rev. Lett.* 88 (2002) 245701. doi:10.1103/PhysRevLett.88.245701.
URL <https://link.aps.org/doi/10.1103/PhysRevLett.88.245701>
- [22] K. R. Elder, M. Grant, Modeling elastic and plastic deformations in nonequilibrium processing using phase field crystals, *Phys. Rev. E* 70 (2004) 051605. doi:10.1103/PhysRevE.70.051605.
URL <https://link.aps.org/doi/10.1103/PhysRevE.70.051605>
- [23] K. Kim, Z. Lee, W. Regan, C. Kisielowski, M. F. Crommie, A. Zettl, Grain boundary mapping in polycrystalline graphene, *ACS Nano* 5 (3) (2011) 2142–2146, pMID: 21280616. arXiv:<http://dx.doi.org/10.1021/nn1033423>, doi:10.1021/nn1033423.
URL <http://dx.doi.org/10.1021/nn1033423>
- [24] Z. Fan, T. Siro, A. Harju, Accelerated molecular dynamics force evaluation on graphics processing units for thermal conductivity calculations, *Computer Physics Communications* 184 (5) (2013) 1414 – 1425. doi:<http://dx.doi.org/10.1016/j.cpc.2013.01.008>.
URL <http://www.sciencedirect.com/science/article/pii/S0010465513000258>
- [25] Z. Fan, L. F. C. Pereira, H.-Q. Wang, J.-C. Zheng, D. Donadio, A. Harju, Force and heat current formulas for many-body potentials in molecular dynamics simulations with applications to thermal conductivity calculations, *Phys. Rev. B* 92 (2015) 094301. doi:10.1103/PhysRevB.92.094301.
URL <https://link.aps.org/doi/10.1103/PhysRevB.92.094301>
- [26] Z. Fan, W. Chen, V. Vierimaa, A. Harju, Efficient molecular dynamics simulations with many-body potentials on graphics processing units, *Computer Physics Communications* 218 (2017) 10 – 16. doi:<https://doi.org/10.1016/j.cpc.2017.05.003>.
URL <http://www.sciencedirect.com/science/article/pii/S0010465517301339>
- [27] J. Tersoff, Modeling solid-state chemistry: Interatomic potentials for multicomponent systems, *Phys. Rev. B* 39 (1989) 5566–5568. doi:10.1103/PhysRevB.39.5566.
URL <https://link.aps.org/doi/10.1103/PhysRevB.39.5566>
- [28] L. Lindsay, D. A. Broido, Optimized tersoff and brenner empirical potential parameters for lattice dynamics and phonon thermal transport in carbon nanotubes and graphene, *Phys. Rev. B* 81 (2010) 205441. doi:10.1103/PhysRevB.81.205441.
URL <https://link.aps.org/doi/10.1103/PhysRevB.81.205441>
- [29] S. Nosé, A unified formulation of the constant temperature molecular dynamics methods, *The Journal of Chemical Physics* 81 (1) (1984) 511–519. arXiv:<http://dx.doi.org/10.1063/1.447334>, doi:10.1063/1.447334.
URL <http://dx.doi.org/10.1063/1.447334>
- [30] W. G. Hoover, Canonical dynamics: Equilibrium phase-space distributions, *Phys. Rev. A* 31 (1985) 1695–1697. doi:10.1103/PhysRevA.31.1695.
URL <https://link.aps.org/doi/10.1103/PhysRevA.31.1695>
- [31] G. J. Martyna, M. L. Klein, M. Tuckerman, Nosé-hoover chains: The canonical ensemble via continuous dynamics, *The Journal of Chemical Physics* 97 (4) (1992) 2635–2643. arXiv:<http://dx.doi.org/10.1063/1.463940>, doi:10.1063/1.463940.
URL <http://dx.doi.org/10.1063/1.463940>
- [32] W. C. Swope, H. C. Andersen, P. H. Berens, K. R. Wilson, A computer simulation method for the calculation of equilibrium constants for the formation of physical clusters of molecules: Application to small water clusters, *The Journal of Chemical Physics* 76 (1) (1982) 637–649. arXiv:<http://dx.doi.org/10.1063/1.442716>, doi:10.1063/1.442716.
URL <http://dx.doi.org/10.1063/1.442716>
- [33] E. S. Landry, A. J. H. McGaughey, Thermal boundary resistance predictions from molecular dynamics simulations and theoretical calculations, *Phys. Rev. B* 80 (2009) 165304. doi:10.1103/PhysRevB.80.165304.
URL <https://link.aps.org/doi/10.1103/PhysRevB.80.165304>
- [34] A. Rajabpour, S. M. V. Allaei, F. Kowsary, Interface thermal resistance and thermal rectification in hybrid graphene-graphane nanoribbons: A nonequilibrium molecular dynamics study, *Applied Physics Letters* 99 (5) (2011) 051917. arXiv:<http://dx.doi.org/10.1063/1.3622480>, doi:10.1063/1.3622480.
URL <http://dx.doi.org/10.1063/1.3622480>
- [35] K. Gordiz, S. M. V. Allaei, Thermal rectification in pristine-hydrogenated carbon nanotube junction: A molecular dynamics study, *Journal of Applied Physics* 115 (16) (2014) 163512. arXiv:<http://dx.doi.org/10.1063/1.4873124>, doi:10.1063/1.4873124.
URL <http://dx.doi.org/10.1063/1.4873124>
- [36] J. K. Bohrer, K. Schrer, L. Brendel, D. E. Wolf, Thermal resistance of twist boundaries in silicon nanowires by nonequilibrium molecular dynamics, *AIP Advances* 7 (4) (2017) 045105. arXiv:<http://dx.doi.org/10.1063/1.4979982>, doi:10.1063/1.4979982.
URL <http://dx.doi.org/10.1063/1.4979982>
- [37] K. Sääskilahti, J. Oksanen, J. Tulkki, S. Volz, Role of anharmonic phonon scattering in the spectrally decomposed thermal conductance at planar interfaces, *Phys. Rev. B* 90 (2014) 134312. doi:10.1103/PhysRevB.90.134312.
URL <https://link.aps.org/doi/10.1103/PhysRevB.90.134312>
- [38] K. Sääskilahti, J. Oksanen, S. Volz, J. Tulkki, Frequency-dependent phonon mean free path in carbon nanotubes from nonequilibrium molecular dynamics, *Phys. Rev. B* 91 (2015) 115426. doi:10.1103/PhysRevB.91.115426.
URL <https://link.aps.org/doi/10.1103/PhysRevB.91.115426>
- [39] K. Sääskilahti, J. Oksanen, J. Tulkki, A. J. H. McGaughey, S. Volz, Vibrational mean free paths and thermal conductivity of amorphous silicon from non-equilibrium molecular dynamics simulations, *AIP Advances* 6 (12) (2016) 121904. arXiv:<http://dx.doi.org/10.1063/1.4968617>, doi:10.1063/1.4968617.
URL <http://dx.doi.org/10.1063/1.4968617>
- [40] Y. Zhou, X. Zhang, M. Hu, Quantitatively analyzing phonon spectral contribution of thermal conductivity based on nonequilibrium molecular dynamics simulations. I. From space Fourier transform, *Phys. Rev. B* 92 (2015) 195204. doi:10.1103/PhysRevB.92.195204.
URL <https://link.aps.org/doi/10.1103/PhysRevB.92.195204>
- [41] Y. Zhou, M. Hu, Quantitatively analyzing phonon spectral contribution of thermal conductivity based on nonequilibrium molecular dynamics simulations. II. From time Fourier transform, *Phys. Rev. B* 92 (2015) 195205. doi:10.1103/PhysRevB.92.195205.
URL <https://link.aps.org/doi/10.1103/PhysRevB.92.195205>

195205

- [42] Z. Fan, L. F. C. Pereira, P. Hirvonen, M. M. Ervasti, K. R. Elder, D. Donadio, T. Ala-Nissila, A. Harju, Thermal conductivity decomposition in two-dimensional materials: Application to graphene, *Phys. Rev. B* 95 (2017) 144309. doi:10.1103/PhysRevB.95.144309.
URL <https://link.aps.org/doi/10.1103/PhysRevB.95.144309>
- [43] T. Feng, W. Yao, Z. Wang, J. Shi, C. Li, B. Cao, X. Ruan, Spectral analysis of nonequilibrium molecular dynamics: Spectral phonon temperature and local nonequilibrium in thin films and across interfaces, *Phys. Rev. B* 95 (2017) 195202. doi:10.1103/PhysRevB.95.195202.
URL <https://link.aps.org/doi/10.1103/PhysRevB.95.195202>
- [44] J. M. Dickey, A. Paskin, Computer simulation of the lattice dynamics of solids, *Phys. Rev.* 188 (1969) 1407–1418. doi:10.1103/PhysRev.188.1407.
URL <https://link.aps.org/doi/10.1103/PhysRev.188.1407>
- [45] E. Pop, V. Varshney, A. K. Roy, Thermal properties of graphene: Fundamentals and applications, *MRS Bulletin* 37 (12) (2012) 1273–1281. doi:10.1557/mrs.2012.203.
- [46] J. E. Turney, A. J. H. McGaughey, C. H. Amon, Assessing the applicability of quantum corrections to classical thermal conductivity predictions, *Phys. Rev. B* 79 (2009) 224305. doi:10.1103/PhysRevB.79.224305.
URL <https://link.aps.org/doi/10.1103/PhysRevB.79.224305>
- [47] T.-H. Liu, S.-C. Lee, C.-W. Pao, C.-C. Chang, Anomalous thermal transport along the grain boundaries of bicrystalline graphene nanoribbons from atomistic simulations, *Carbon* 73 (2014) 432 – 442. doi:http://dx.doi.org/10.1016/j.carbon.2014.03.005.
URL <http://www.sciencedirect.com/science/article/pii/S0008622314002474>
- [48] C.-W. Nan, R. Birringer, D. R. Clarke, H. Gleiter, Effective thermal conductivity of particulate composites with interfacial thermal resistance, *Journal of Applied Physics* 81 (10) (1997) 6692–6699. arXiv:http://dx.doi.org/10.1063/1.365209, doi:10.1063/1.365209.
URL <http://dx.doi.org/10.1063/1.365209>